Springer

Journal of Mechanical Science and Technology 23 (2009) 3436~3447

Journal of Mechanical Science and Technology

www.springerlink.com/content/1738-494x
DOI 10.1007/s12206-009-0924-0

# Linear stability analysis of acoustically driven pressure oscillations in a lean premixed gas turbine combustor †

Kyu Tae Kim* and Domenic Santavicca

*Propulsion Engineering Research Center, Department of Mechanical and Nuclear Engineering, The Pennsylvania State University, University Park, PA, 16802, USA*

(Manuscript Received May 13, 2009; Revised July 10, 2009; Accepted July 28, 2009)

**Abstract**

The dynamic response of a turbulent premixed flame to acoustic velocity perturbations was experimentally determined in a swirl-stabilized lean-premixed gas turbine combustor. CH* chemiluminescence intensity and the two-microphone method were used to measure heat release rates and inlet velocity fluctuations, respectively. Using the n-τ formulation, gain and phase of flame transfer functions were incorporated into an analytic thermoacoustic model to predict instability frequencies and modal structures. Self-excited instability measurements were performed to verify eigenfrequencies predicted by the thermoacoustic model. Instability frequency predicted by the model is supported by experimental results. Results show that the self-excited instability frequency of ~ 220 Hz results from the fact that the flames amplify flow perturbations with $f$ = 150 ~ 250 Hz. The other instability frequency of ~ 350 Hz occurs because the whole combustion system has an eigenfrequency corresponding to the ¼-wave eigenmode of the mixing section.

***Keywords*:** Combustion instabilities; Flame transfer function; Gas turbine; Lean premixed; Linear stability analysis

## 1. Introduction

In order to meet strict emission regulations, lean-premixed, pre-vaporized (LPP) technology has been adopted for many industrial applications because it reduces the maximum flame temperature, leading to significant reduction of thermal $NO_x$. Unfortunately, lean premixed flames are susceptible to combustion instability. Combustion instability generally refers to the periodic, high-amplitude pressure fluctuations in a combustion chamber due to the resonant coupling between the system acoustics and the unsteady heat release. Combustion instability is by nature related to the energy conversion of thermal to acoustic energy, leading to a self-excited feedback loop. These high amplitude pressure oscillations can substantially reduce performance of a system, and can also destroy part of engines. A number of experimental, theoretical, and numerical studies have been performed to identify and understand underlying instability driving mechanisms, and also to predict and control the occurrence of instabilities [1-3]. It is still difficult to accurately predict instability characteristics at the development stage, however. The response of flames to flow perturbations caused by the pressure waves in a combustor is critical information in the theoretical description of combustion-induced oscillations.

For a perfectly premixed flame, the response of a flame can be determined by means of the flame transfer function, where the input function is acoustic velocity fluctuation and the output function is heat release rate oscillation. In general, the flame transfer function is expressed by the ratio of the fluctuating components of output to the input functions, normalized by their corresponding time-averaged values:

† This paper was recommended for publication in revised form by Associate Editor Tong Seop Kim

*Corresponding author. Tel.: +44 (0)1223 764474, Fax.: 44 (0)1223 765321
E-mail address: ktk23@cam.ac.uk

$$FTF(f) = \frac{Q'(f)/\overline{Q}}{V'(f)/\overline{V}} \quad (1)$$

The flame transfer function can be obtained by experimental methods [4-7], theoretical approaches [8-10], and unsteady CFD calculations [11-13]. Experimental determination of forced flame response is reliable, and it is also required to validate FTF derived theoretically and numerically.

Experimental investigations of the response of a turbulent flame to inlet velocity oscillations and/or equivalence ratio fluctuations have confirmed the underlying mechanisms for nonlinear response and the dynamics of forced flames with respect to changes in inlet operating conditions [4-7]. Applications of FTF measurements to prediction of eigenfrequencies and modal structures of self-excited instabilities have been explored [14, 15]. If the FTF were available, then reduced-order flame response models could be used to predict the onset of instabilities [16, 17]. The FTF can also be used in thermoacoustic network modeling, where the FTF provides a source term, i.e., unsteady heat release in a combustion chamber. Poinsot & Veynante [18] described a general method for one-dimensional thermoacoustic modeling to predict eigenfrequency and corresponding eigenmode.

In the present paper, a methodology to predict self-induced instability frequency in a lean-premixed gas turbine combustor is described. Flame transfer functions of a turbulent premixed flame are experimentally determined. The gain and phase of the FTF are mathematically formulated by using the n-τ model, and they are incorporated into a theoretical thermoacoustic model to predict eigenfrequencies and modal structures. Predicted eigenfrequencies are validated by self-excited flame response measurements. Analytic thermoacoustic modeling and experimental determination of FTF are utilized to interpret self-induced pressure oscillations observed in a lean-premixed, gas turbine combustor.

## 2. Experimental methods

Fig. 1 shows a schematic of a lean-premixed, variable-length, gas turbine combustor facility, used in these experiments. This facility consists of an air inlet section, a siren, a mixing section, an optically-accessible quartz combustor section, a steel combustor section, and an exhaust section. A siren-type modulation device is used to provide acoustic modulations. The siren is driven by a variable-speed DC motor, thus providing capabilities for changing forcing frequency (~ 400 Hz). The amplitude of acoustic velocity perturbation ($V'/V_{mean}$) can be varied by controlling the relative amount of air/fuel flow through the modulating device. At the entrance to the mixing section the flow is choked. This provides a well-defined acoustic boundary condition for self-excited flame response measurements. For forced flame response measurements, the choking plate is removed and mounted upstream of the siren. The fuel is injected and mixed far upstream of the choked inlet to create spatially and temporally homogeneous reactant mixtures before they enter a reaction zone.

The combustor consists of a stainless steel dump plane, to which an optically accessible fused-silica combustor with a 109.2 mm-diameter and 334.8 mm-length is attached. The downstream end of the quartz combustor is connected to a stainless steel variable-length combustor section. The length of the combustor can be continuously varied between 762 mm and 1524 mm by moving a water-cooled plug along the length of the steel combustor section. The overall combustor length is defined as the distance from the combustor dump plane to the plug. Detailed dimensions are included in Fig. 1.

PCB 112A04 piezoelectric transducers with charge amplifiers are used to measure unsteady pressure perturbations in the mixing and the combustor sections. Two pressure transducers located at 12.7 mm and 50.8 mm upstream of the combustor dump plane are used to estimate the inlet velocity fluctuations using the two-microphone method [19, 20]. To calibrate the two-microphone method, direct measurements of velocity fluctuations are performed under cold flow conditions with a TSI 1210-20 const-ant temperature hot wire anemometer. A photomultiplier tube (PMT, Hamamatsu model H7732-10) is used to

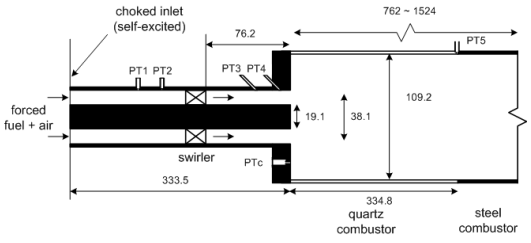


Fig. 1. Schematic of a swirl-stabilized, lean-premixed, gas turbine combustor. Dimensions in millimeters.

measure the global CH* (432 ± 5 nm) chemiluminescence emission intensities from a whole flame. An ICCD camera (Princeton Instruments model 576G) with a CH* band pass filter centered at 430 nm (10 nm FWHM) is used to record the flame images. For phase-averaged imaging, the ICCD camera is synchronized with the combustor pressure signal and fifty averaged images are taken over a cycle of oscillation with a phase interval of 30°. The phase angle φ = 0° corresponds to the positive-to-negative zero transition, and φ = 270° to the maximum combustor pressure. The field of view of the photomultiplier and the ICCD camera is such that they cover the entire combustion zone, and it is ensured that the PMT views the same region. A three-point Abel deconvolution procedure is used to reconstruct the two-dimensional structure of the flame from the line-of-sight integrated CH* chemiluminescence images.

All tests were performed at a mean pressure of 1 atm and at mean equivalence ratios ranging from 0.55 to 0.70. The range of equivalence ratio represents typical values of equivalence ratio in real lean-premixed gas turbine engines. For the present study, modulation frequencies were varied from 100 to 400 Hz, which includes self-sustained instability frequencies observed in the rig, shown in Fig. 1. To reduce the influence of the system's acoustics on upstream forcing, the combustor length was kept the shortest, 0.584 m. At this condition, resonance frequency of the system is much higher than the forcing frequency and therefore the resonant effects are minimized. The fuel was pure natural gas or a mixture of natural gas and $H_2$ by volume. The full list of operating conditions and fuel compositions is given in Table 1.

Experimental data were obtained with a National Instruments data acquisition system controlled by Labview software. 16,384 data points were taken at a sampling rate of 8192 Hz, which resulted in a frequency resolution of 0.5 Hz and a time resolution of 0.122 msec. Spectral analysis of the signals was performed using the fast Fourier transform (FFT) technique.

Table 1. Test conditions for forced (self-excited) flame response measurements.

| Parameters | Test conditions |
|---|---|
| pressure (P) | 1 atm |
| inlet temperature ($T_{in}$) | 200 °C |
| nozzle velocity ($V_{mean}$) | 60, 70, 80, 90, 100 m/s |
| equivalence ratio (Φ) | 0.55, 0.60, 0.65, 0.70 |
| forcing frequency ($f$) | 100 ~ 400 Hz ($\Delta f$ = 25 Hz) |
| forcing amplitude ($V'/V_{mean}$) | up to 0.60 |
| fuel composition ($X_{H2}$) | 0.00, 0.15, 0.30, 0.45 |

## 3. Linear stability analysis

Thermoacoustic systems can be modeled efficiently as networks of acoustic elements, where each element corresponds to a certain component of the system [21]. Fig. 2 shows a combustion system modeled as an ensemble of acoustic sub-elements. The whole combustor can be decomposed into acoustic sub-elements such as the mixing section, the swirler, the flame, and the combustor. However, in this model the swirler is not taken into account, because its influence on the acoustic field in the mixing section is negligible. This is because acoustic pressure measurements up- and downstream of the swirler using PT1 through PT4 shown in Fig. 1 confirmed that amplitude and phase of pressure waves are not significantly affected by the existence of the swirler; that is, the swirler is acoustically transparent.

According to linear acoustic theory, governing equations for acoustic velocity and pressure in low-speed reacting flows can be expressed in the following equations [18]:

$$\frac{\partial u'}{\partial t}+\frac{1}{\rho_0}\frac{\partial p'}{\partial x}=0 \tag{2}$$

$$\frac{1}{\gamma p_0}\frac{\partial p'}{\partial t}+\frac{1}{S}\frac{\partial (Su')}{\partial x}=\frac{\gamma-1}{\gamma p_0}\dot{q}_T' \tag{3}$$

where $\rho_0 = \rho_0(x)$ is the mean density; $S = S(x)$ is the cross-sectional area; $\gamma$ is the specific heat ratio; $\dot{q}_T'$

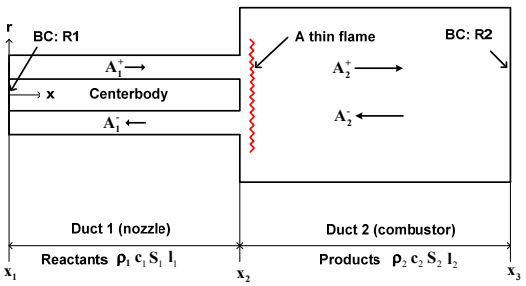


Fig. 2. Decomposition of the combustor into three acoustic sub-elements.

is the unsteady heat release rate [W/m$^3$]. Integrating Eqs. (2) and (3) from $x_2^-$ to $x_2^+$ and taking the limit where $x_2^-$ and $x_2^+$ go to $x_2$, acoustic jump conditions for a thin flame can be obtained.

$$p'(x_2^+) = p'(x_2^-) \tag{4}$$

$$S(x_2^+)u'(x_2^+) - S(x_2^-)u'(x_2^-) = \frac{\gamma - 1}{\gamma p_0}\dot{Q}_T' \tag{5}$$

Assuming harmonic variation of any acoustic variable, the acoustic pressure and velocity in ducts 1 and 2 may be expressed in the following forms:

$$p_1' = \hat{p}_1 e^{-i\omega t} = A_1^+ e^{ik_1(x-x_1)-i\omega t} + A_1^- e^{-ik_1(x-x_1)-i\omega t} \tag{6}$$

$$u_1' = \hat{u}_1 e^{-i\omega t} = \frac{A_1^+}{\rho_1 c_1} e^{ik_1(x-x_1)-i\omega t} - \frac{A_1^-}{\rho_1 c_1} e^{-ik_1(x-x_1)-i\omega t} \tag{7}$$

$$p_2' = \hat{p}_2 e^{-i\omega t} = A_2^+ e^{ik_2(x-x_2)-i\omega t} + A_2^- e^{-ik_2(x-x_2)-i\omega t} \tag{8}$$

$$u_2' = \hat{u}_2 e^{-i\omega t} = \frac{A_2^+}{\rho_2 c_2} e^{ik_2(x-x_2)-i\omega t} - \frac{A_2^-}{\rho_2 c_2} e^{-ik_2(x-x_2)-i\omega t} \tag{9}$$

Substituting Eqs. (6)-(9) into Eqs. (4) and (5), and assuming harmonic time dependence of the unsteady heat release, $\dot{Q}_T' = \hat{\dot{Q}} e^{-i\omega t}$,

$$A_2^+ + A_2^- = A_1^+ e^{ik_1 l_1} + A_1^- e^{-ik_1 l_1} \tag{10}$$

$$\frac{S_2}{\rho_2 c_2}(A_2^+ - A_2^-) = \frac{S_1}{\rho_1 c_1}(A_1^+ e^{ik_1 l_1} - A_1^- e^{-ik_1 l_1}) + \frac{\gamma - 1}{\gamma p_0}\hat{\dot{Q}} \tag{11}$$

A section parameter, which represents the ratio of the acoustic impedances at the interface of ducts 1 and 2, can be defined as Eq. (12).

$$\Gamma_1 = \frac{\rho_2 c_2 S_1}{\rho_1 c_1 S_2} \tag{12}$$

Rearranging Eqs. (10) and (11) using (12) as a matrix form, we can get the following equation:

$$\begin{pmatrix} A_2^+ \\ A_2^- \end{pmatrix} = \frac{1}{2}\begin{bmatrix} e^{ik_1 l_1}(1+\Gamma_1) & e^{-ik_1 l_1}(1-\Gamma_1) \\ e^{ik_1 l_1}(1-\Gamma_1) & e^{-ik_1 l_1}(1+\Gamma_1) \end{bmatrix}\begin{pmatrix} A_1^+ \\ A_1^- \end{pmatrix} + \frac{1}{2}\frac{\rho_2 c_2}{S_2}\frac{\gamma - 1}{\rho_1 c_1^2}\begin{pmatrix} \hat{\dot{Q}} \\ -\hat{\dot{Q}} \end{pmatrix} \tag{13}$$

Let's consider the boundary conditions. From Eqs. (6) to (9),

$$\frac{A_1^+}{A_1^-} = R_1 \tag{14}$$

$$\frac{A_2^+}{A_2^-} e^{2ik_2 l_2} = R_2 \tag{15}$$

$R_1$ and $R_2$ denote the reflection coefficients at the inlet and outlet boundaries. Eq. (13) and its BC's (14) and (15) lead to a linear system which has a non-trivial solution only for a limited set of angular frequency. To close the system, however, the unsteady heat release should be provided. It can be obtained from analytic, experimental, and numerical simulation methods. Here, flame transfer function measurements are used by means of the classical n-τ model. The flame transfer function is defined as

$$F(\omega) = \frac{\hat{\dot{Q}}/\bar{\dot{Q}}}{\hat{u}/\bar{u}} \tag{16}$$

The flame transfer function is cast in the following form:

$$F(\omega) = \frac{\hat{\dot{Q}}/\bar{\dot{Q}}}{\hat{u}/\bar{u}} = n(\omega)e^{i\omega\tau} \tag{17}$$

Gain and phase are modeled separately. Gain can be modeled as a second order function to represent the overshoot behavior as can be seen later, and phase typically linearly increases with frequency.

$$\Delta\varphi = \omega\tau \tag{18}$$

$$n(\omega) = \left| \frac{K}{1 + i2\xi(\omega/\omega_c) - (\omega/\omega_c)^2} \right| \tag{19}$$

The constants τ, ξ, K, and $\omega_c$ are determined from empirical fits of Eqs. (18) and (19). Substituting Eq. (17) into Eq. (13) and after some manipulation, we get the dispersion relation:

$$\frac{1}{R_2}\left(1+\Gamma_1+\Gamma_2 ne^{i\omega\tau}\right)+\frac{1}{R_1R_2}e^{-2ik_1l_1}$$
$$\times\left(1-\Gamma_1-\Gamma_2 ne^{i\omega\tau}\right)-e^{-2ik_2k_2}\left(1-\Gamma_1-\Gamma_2 ne^{i\omega\tau}\right)$$
$$-\frac{1}{R_1}e^{-2i(k_1l_1+k_2l_2)}\left(1+\Gamma_1+\Gamma_2 ne^{i\omega\tau}\right)=0 \quad (20)$$

$$\Gamma_2=\frac{\rho_2c_2}{\rho_1c_1S_2}\frac{\gamma-1}{\rho_1c_1^2}\frac{\overline{Q}}{\overline{u}} \quad (21)$$

Eq. (20) determines the eigenfrequencies of the system by solving for the real and imaginary parts of the complex angular frequency, ω. If the imaginary part of ω is positive, the solution is unstable and combustion instability is expected. The instability frequency is obtained from the real part of ω. This linear stability analysis can be extended to capture nonlinear features of self-sustained instability using flame describing functions.

## 4. Results and discussion

### *4.1 Flame transfer function measurement*

Fig. 3 shows the amplitude dependence of the normalized heat release response and the phase of the flame transfer function at a modulation frequency of 100 Hz. Measurements of CH* chemiluminescence emission intensities are used as an indicator of heat release rate oscillations. For all levels of inlet velocity modulation, the coherence between inlet velocity and chemiluminescence signals at the forcing frequency was close to unity, enabling flame transfer functions to be accurately measured. It can be observed from Fig. 3 that the normalized heat release response linearly increases with the forcing amplitude, up to $V'/V_{mean} \sim 0.370$. The maximum driving amplitude point is not caused by flame blowoff, but by a limitation of the modulating device. The gain is nearly constant with respect to the forcing amplitude, representing the linear flame response. The flame is stretched or contracted without shear layer rollup. The phase of the flame transfer function is nearly independent of the forcing amplitude, implying that the center of heat-release (maximum heat release location) is not affected by forcing amplitude. However, as shown in Fig. 4, the response of the flame at the forcing frequency of 200 Hz clearly shows the nonlinear characteristic. The normalized CH* chemiluminescence intensity saturates at the modulation amplitude of $V'/V_{mean} \sim 25\%$, where the flame response was linear

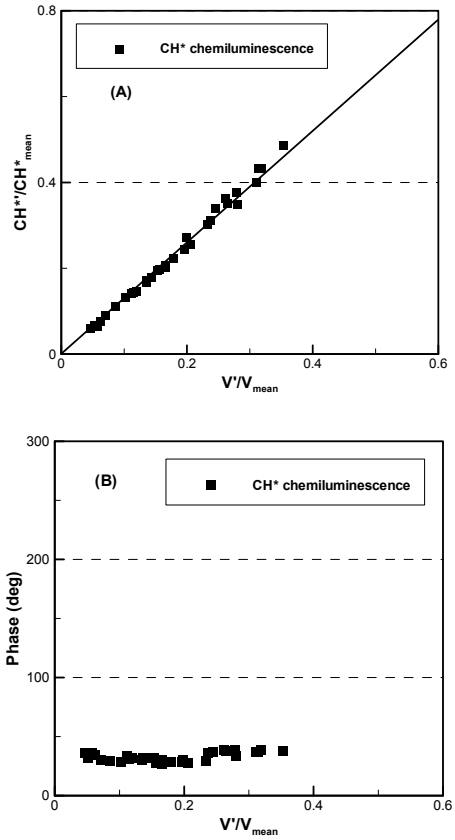


Fig. 3. (A) Normalized heat release response ($CH^{*\prime}/CH^*_{mean}$) and (B) phase of flame transfer function at a modulation frequency of 100 Hz, plotted as a function of forcing amplitude. Inlet conditions: $T_{in}$ = 200 °C, $V_{mean}$ = 60 m/s, Φ = 0.60, and $X_{H2}$ = 0.00.

for the modulation at 100 Hz. Note that the phase of the flame transfer function is independent of perturbation amplitude, irrespective of the nonlinear response of the flame.

It is known that this saturation phenomenon is related to a nonlinear evolution of the flame surface area [4-6]. In particular, the minimum level of the inception of the nonlinear flame response decreases with increasing modulation frequency [6, 22]. Several factors affect nonlinear flame dynamics: unsteady flame liftoff [23, 24], local/global extinction [23, 25], equivalence ratio oscillation [26], and shear layer rollup [4, 5, 22]. Because an understanding of a combustor's nonlinear dynamics is critical to the prediction of the limit-cycle oscillation amplitude and nonlinear processes of mode switching and instability triggering, the nonlinear response of turbulent premixed flames has been examined.

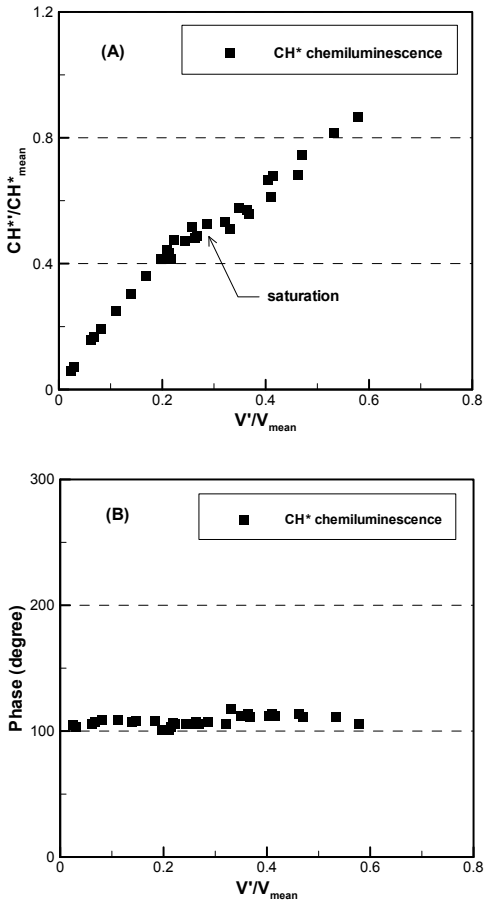


Fig. 4. (A) Normalized heat release response ($CH^{*\prime}/CH^{*}_{mean}$) and (B) phase of flame transfer function at a modulation frequency of 200 Hz, plotted as a function of forcing amplitude. Inlet conditions: $T_{in}$ = 200 °C, $V_{mean}$ = 60 m/s, Φ = 0.60, and $X_{H2}$ = 0.00.

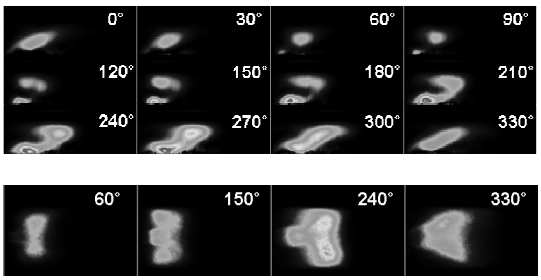


Fig. 5. (A) Phase-synchronized CH* chemiluminescence images at a modulation frequency of 200 Hz and $V'/V_{mean}$ = 25%. (B) Line-of-sight integrated, background-corrected CH* chemiluminescence images at φ = 60, 150, 240, 330°. Inlet conditions: $T_{in}$ = 200 °C, $V_{mean}$ = 60 m/s, Φ = 0.60, and $X_{H2}$ = 0.00.

Deconvoluted and line-of-sight integrated phase-averaged CH* chemiluminescence images at a modulation frequency of 200 Hz and amplitude of $V'/V_{mean}$ = 25% are shown in Fig. 5. In the deconvoluted image, only the upper half is shown, because the flame is symmetrical. All input conditions are the same as for Fig. 4. It is noteworthy that at the condition considered here, the flame front bends toward the inner recirculation zone at φ = 270°. The interaction between a vortex-ring structure and the flame is significant at φ = 180° ~ 300°. In particular, line-of-sight integrated images at φ = 150° and 240° clearly show rollup of the shear layer and convection in the flow direction, respectively. The shear layer rollup shortens the flame length, which in turn decreases the flame area in a nonlinear manner. Hence, the gain of FTF decreases in the nonlinear regime, as shown in Fig. 4 (A).

### *4.2 n-τ formulation*

Fig. 6 presents the gain and phase of FTF at a constant forcing amplitude, $V'/V_{mean}$ = 0.100. The flame response at this level of modulation remains in the linear regime. With increasing the modulation frequency, the gain increases and reaches its maximum value at $f$ = 225 Hz. Then, the gain gradually decreases close to zero in the high frequency limit. The gain of FTF exhibits an overshoot which is also observed in other studies [4, 14, 27]. The phase evolves quasi-linearly with modulation frequency. Also, the phase and the gain are empirically fitted using Eqs. (18) and (19), as shown in Fig. 6. From these fitting, the following parameter values are obtained: ξ = 0.367, $\omega_c$ = 1730, K = 1.000 and τ = 2.18 msec. These values are found to be strongly dependent on fuel composition [27]. These parameters are substituted into Eq. (20) to solve for complex eigenvalues of the system.

### *4.3 Eigenfrequency prediction*

Mean temperatures in each section were assumed to be constant, and thermodynamic properties of fresh and burnt gases were calculated by the ideal gas law. The combustor temperature, $T_2$ was assumed to be the adiabatic flame temperature ($T_{ad}$ = 1320 °C). The downstream end of the combustor, $R_2$ = 1, was assumed to be a velocity node point, but the inlet boundary condition, $R_1$ = 0.212*exp (-i*0.410), was obtained from self-induced instability measurements.

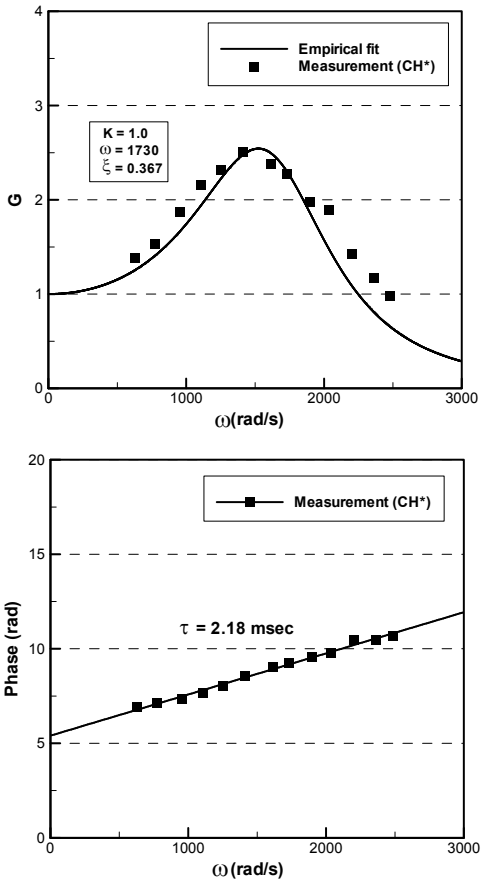


Fig. 6. Gain and phase difference of the flame transfer function and their corresponding empirical fits. Inlet conditions: $T_{in}$ = 200 °C, $V_{mean}$ = 60 m/s, Φ = 0.60, $X_{H2}$ = 0.00, and $V'/V_{mean}$ = 0.100.

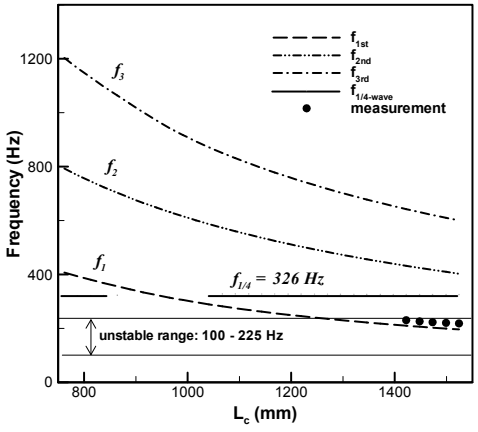


Fig. 7. Eigenfrequencies calculated by thermoacoustic model and self-excited instability frequencies (measurement) as a function of the combustor length. Inlet conditions: $T_{in}$ = 200 °C, $V_{mean}$ = 60 m/s, Φ = 0.60, and $X_{H2}$ = 0.00.

With these boundary conditions, experimentally determined flame transfer functions were incorporated into the thermoacoustic model to solve the dispersion relation. Eq. (20) was numerically solved using Nelder-Mead Simplex method. The combustor length, $l_2$, was used as a bifurcation parameter.

Fig. 7 shows eigenfrequencies calculated by the thermoacoustic model and measurement results (symbols). The three curves, $f_1$, $f_2$, and $f_3$, correspond to the lowest three longitudinal mode eigenfrequency as a function of the combustor length. The longer the combustor length, the lower the eigenfrequencies. Also, shown as a horizontal line ($f$ = 326 Hz) in the Fig. 7 is the calculated ¼-wave resonant frequency of the mixing section at the given inlet temperature, $T_{in}$ = 200 °C, which is independent of the combustor length. It is interesting to note that the ¼-wave eigenmode does not occur at the combustor length of 850 mm < $L_c$ < 1040 mm, presumably because the ¼-wave eigenmode competes with the first longitudinal mode, $f_1$, and therefore, only one eigenmode is selected. At this operating condition, the strongest self-excited instability was observed at $L_c$ = 1524 mm ($f$ = 219 Hz and $P_c'/P_{c,\,mean}$ = 0.0534). Eigenfrequencies predicted by the analytic model agree well with experimental measurements, and the observed eigenmode corresponds to the first longitudinal mode.

To determine the range of instability frequencies, the time-lag model was used. With a choked inlet, pressure leads velocity by 90° at the combustor dump plane. Therefore, the first unstable regime is determined by 0.75 < τ/T < 1.25. Fig. 8 presents the ratio

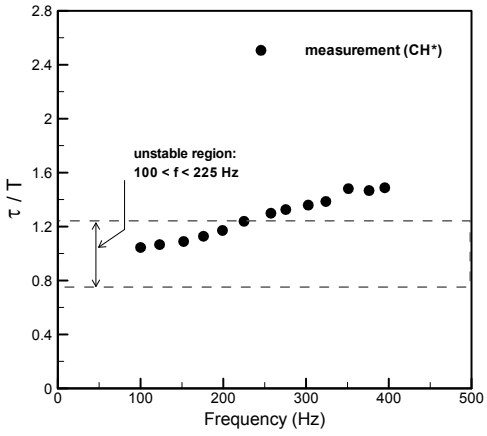


Fig. 8. The ratio of convection time to the acoustic period vs. forcing frequency. Inlet conditions: $T_{in}$ = 200 °C, $V_{mean}$ = 60 m/s, Φ = 0.60, and $X_{H2}$ = 0.00.

of the convection time to the acoustic period vs. forcing frequency at the same operating condition, showing that unstable frequency range is between 100 Hz and 225 Hz. The convection time delay was calculated from the phase information of FTF.

Applying this unstable frequency range to the result of thermoacoustic modeling, as shown in Fig. 7, instability frequency prediction by the thermoacoustic model and the time-lag analysis shows good agreement with measured instability frequency band.

### *4.4 Self-excited instability measurement*

To verify thermoacoustic model predictions, self-excited flame response measurements were characterized in a lean-premixed, variable-length, gas turbine combustor facility, shown in Fig. 1. The capability to vary the combustor length enables to control the acoustic eigenfrequencies of the combustion system at a given operating condition. Fig. 9 shows the dependence of the instability frequency upon the combustor length. It should be noted that the cases where the intensity of instability is strongest are presented for each operating condition, even though the instabilities occur over a certain range of combustor length. Two instability frequency bands are observed. Regime "A" corresponds to $f \sim 220$ Hz at $L_c \sim 1500$ mm, and regime "B" corresponds to $f \sim 350$ Hz at $L_c \sim 1040$ mm. No instability was observed at $L_c < 965$ mm and 1143 mm $< L_c <$ 1346 mm.

In order to interpret the reasons why the coupling between the system acoustics and convection of flow perturbations occurs at only $f \sim 220$ Hz and $f \sim 350$ Hz, the dependence of self-excited instability frequency upon the modulation frequency, where the gain of FTF reaches its maximum value, is shown in Fig. 10. The regime "A" (the lower box) denotes the self-induced instability frequencies, which is consistent with forcing frequencies. We observed that the modulation frequency in which the flame response is relatively strong is 150 ~ 250 Hz, regardless of operating conditions [27]. This means that the flame has a preferred range of frequency where its response is maximum. Meanwhile, regime "B" (the upper box) corresponds to the ¼-wave eigenfrequency of the mixing section, already shown in Fig. 7. Although standing waves are not developed in the mixing section, the combustion system has the eigenfrequency corresponding to the ¼-wave resonance frequency of the mixing section. Hence, at certain

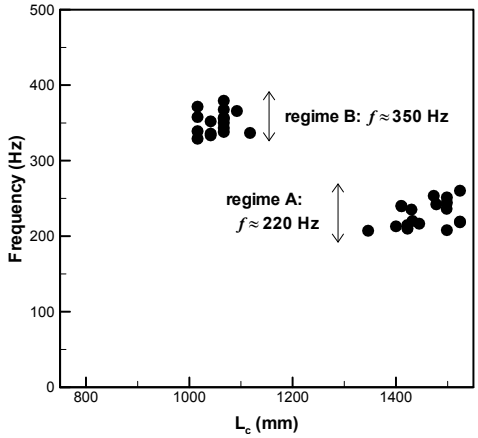


Fig. 9. Dependence of self-excited instability frequency upon the combustor length. Note that the cases where the intensity of instability is strongest are presented for each operating condition. Inlet conditions: $T_{in}$ = 200 °C, $V_{mean}$ = 60, 70, 80, 90 m/s, $\Phi$ = 0.55, 0.60, 0.65, 0.70, and $X_{H2}$ = 0.00, 0.15, 0.30, 0.45.

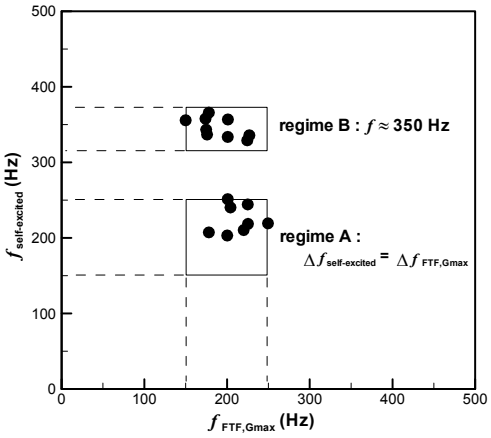


Fig. 10. Dependence of self-excited instability frequency upon the modulation frequency, where the gain reaches its maximum value. Inlet conditions: $T_{in}$ = 200 °C, $V_{mean}$ = 60, 70, 80 m/s, $\Phi$ = 0.55, 0.60, 0.65, 0.70, and $X_{H2}$ = 0.00, 0.15, 0.30, 0.45.

operating conditions, the 1/4-wave eigenmode of the mixing section is excited by the unsteady combustion process, leading to self-sustained pressure oscillations. Similar observation has been reported by Garcia et al. [28]. They reported that an eigenmode of a system was associated with a resonance of the supply plenum. An analytic thermoacoustic model provides infinite number of eigenfrequencies at a given condition, but only selected eigenfrequencies are excited in measurements.

Combustion instability occurs when periodic disturbance convection process couples with acoustic eigenmodes of the combustor. Acoustic eigenfrequencies are determined by speed of sound and the length between the combustor dump plane and the exit of the combustor. However, the convection process is governed by input parameters and the geometry of the nozzle. The distance between the edge of the centerbody and the maximum CH* chemiluminescence intensity location plays a critical role in combustion instability, since the convection time scale is determined by the distance, $L_{CH^*max}$ [27, 29-30]. Fig. 11 plots the dependence of instability frequencies upon effective flame length, $L_{CH^*max}$. The instability frequency is divided into three distinct regimes. In regime 1, the instability frequency is approximately 350 Hz at $L_{CH^*max} < 65$ mm. In regime 3, however, the instability frequency of $f \sim 220$ Hz was observed at $L_{CH^*max} > 85$ mm. This indicates that flames with short flame length can excite high-frequency eigenmodes of the system. In the intermediate range, regime 2, both instability frequencies were measured. Flames in regime 2 can couple with both eigenmodes of the system. This indicates that the flame length is an important parameter playing a critical role in determining self-excited instability frequencies among infinite number of acoustic eigenfrequencies of a system. Also, the flame length was found to be one of relevant parameters controlling the forced response of swirl-stabilized, turbulent premixed flames [27].

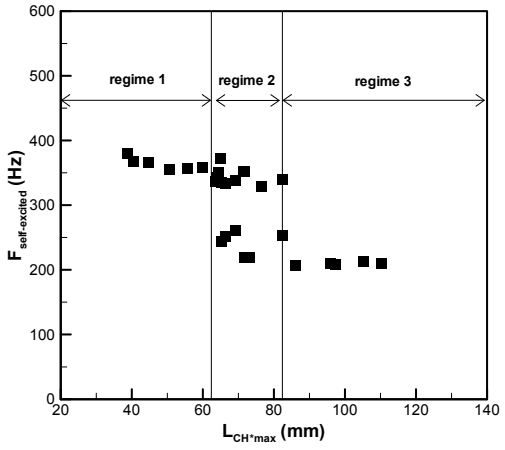


Fig. 11. Dependence of self-excited instability frequency upon flame length, $L_{CH^*max}$. Inlet conditions: $T_{in}$ = 200 °C, $V_{mean}$ = 60, 70, 80, 90 m/s, Φ = 0.55, 0.60, 0.65, 0.70, and $X_{H2}$ = 0.00, 0.15, 0.30, 0.45.

To analyze the relationship between the self-induced instability frequency and the effective flame length, convection time scales were utilized. The phase of the flame transfer function provides convection times needed for the flame to respond to upstream disturbance. The overall time delay consists of a characteristic time delay for the convective transport of the fuel/air mixture from the combustor inlet to the reaction zone, a time delay for the heating of the mixture to ignition temperature, and a characteristic kinetic time delay for the chemical reaction [30]. The phase of the flame transfer function includes these three characteristic time scales. An example of the phase and the convection time with respect to equivalence ratio is presented in Fig. 12. It can be observed that the phase difference increases almost linearly with modulation frequency and increases with decreasing equivalence ratio at a given modulation frequency. This result indicates that the phase difference between acoustic velocity and heat release perturbations is significantly dependent on flame length. Note that the convection time is not linearly related to frequency. It levels off when frequency is greater than 300 Hz. The convection time scales ($\tau_{conv}$) obtained from the flame transfer function measurements were used to normalize the self-induced instability frequency. Fig. 13 shows the normalized instability frequency plotted against the normalized effective flame length, $L_{CH^*max}/R$, where R is the radius of the combustion chamber. These results show that a functional relationship between the two nondimensional parameters exists, and consequently suggest that if the convection time scale and the effective flame length are given, the frequency of limit-cycle pressure oscillations can be predicted.

In the present study, flame transfer functions subjected to infinitesimally small (linear) perturbations were used in a linear stability analysis to predict eigenfrequencies, mode structures, and initial growth rates. In real gas turbine engines, the peak-to-peak magnitude of dynamic pressure oscillations increases exponentially with respect to time and then reaches the limit-cycle amplitude of self excited oscillations. The limit-cycle oscillations are associated with the nonlinear combustor processes, and these processes are primarily governed by the heat release nonlinearity. The nonlinear flame dynamics therefore play a key role in inducing the limit-cycle pressure oscillations. The nonlinear characteristics of a given system cannot be predicted by the linear stability model.

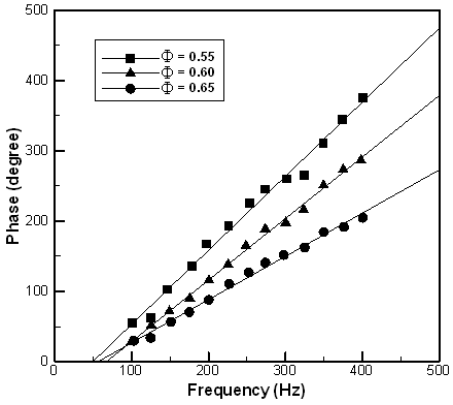


(a)

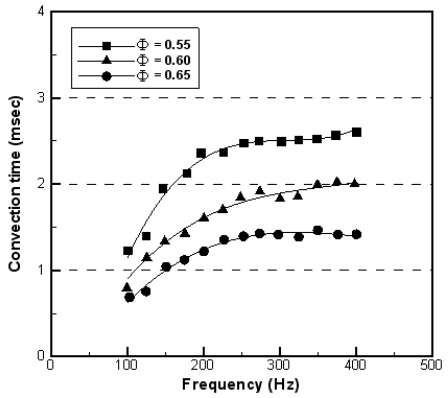


(b)

Fig. 12. (A) Dependence of the phase of the flame transfer functions upon overall equivalence ratio. (B) The corresponding convection time delay with respect to modulation frequency. Inlet conditions: $T_{in}$ = 200 °C, $V_{mean}$ = 60 m/s, $X_{H2}$ = 0.00, and Φ = 0.55, 0.60, 0.65.

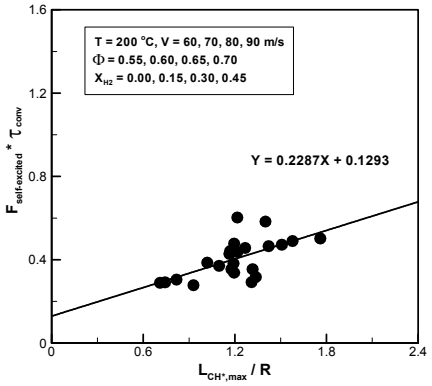


Fig. 13. The normalized self-induced instability frequency ($f_{self\text{-}excited}*\tau_{conv}$), plotted against the normalized effective flame length ($L_{CH*max}/R$). Inlet conditions: $T_{in}$ = 200 °C, $V_{mean}$ = 60, 70, 80, 90 m/s, Φ = 0.55, 0.60, 0.65, 0.70, and $X_{H2}$ = 0.00, 0.15, 0.30, 0.45.

However, the approaches outlined in the present article can be extended to predict the limit-cycle oscillation amplitude and nonlinear processes of mode switching and instability triggering, using nonlinear flame transfer functions [31].

## 5. Conclusions

Flame transfer function measurements were taken in a lean-premixed, swirl-stabilized, gas turbine combustor. The forced response of turbulent premixed flames was incorporated into an analytic thermoacoustic model to predict eigenfrequencies of the system. Predictions showed a good agreement with measurement results. Theoretical models improve our understanding of combustion instability in lean premixed combustors. Particularly, it was shown that the instability frequency of $f$ ~ 220 Hz observed in self-excited flame response measurements corresponds to the modulation frequency, where gain of FTF is highest. The other instability frequency of $f$ ~ 350 Hz corresponds to the ¼-wave eigenmode frequency of the mixing section. Although the flame response is relatively weak at this frequency, the resonance in the mixing section strengthens the self-excited instability. The detailed measurements discussed in this paper are critical to the formulation and identification of eigenmodes of the combustion system, and to improving our understanding of the response of swirled flame to acoustic velocity perturbations.

## Acknowledgment

The authors gratefully acknowledge the financial support of this work by the US-DOE, Grant No. DE-FG26-07NT43069.

## Nomenclature

A : Complex amplitude of pressure waves
c : Speed of sound
f : Forcing frequency
FTF, F : Flame transfer function
FWHM : Full width at half maximum
i : $\sqrt{-1}$
k : Wave number
K : Constant
l, L : Length of ducts
n : Gain of flame transfer function
P : Pressure
PMT : Photomultiplier tube

PT : Pressure transducer
Q, q : Heat release
r : Coordinate in radial direction
R : Reflection coefficient, radius
S : Cross-sectional area
TMM : Two-microphone method
V, u : Velocity
V : Volume
t : Time
T : Period, temperature
x : Coordinate in axial direction
X : Mole fraction

### *Greek symbols*

$\tau$ : Time delay
$\Phi$ : Equivalence ratio
$\varphi$ : Phase difference
$\rho$ : Density
$\gamma$ : Specific heat ratio
$\omega$ : Angular frequency
$\Gamma_1$ : Section parameter
$\Gamma_2$ : Constant
$\xi$ : Damping coefficient
$\Delta$ : Difference
$\lambda$ : Wavelength

### *Overscripts*

$\hat{}$ : Fluctuation amplitude
$\bar{}$ : Mean quantity
$\cdot$ : Time rate of change

### *Superscripts*

+, - : Down- and upward propagating
` : Perturbation quantity

### *Subscripts*

1, 2 : Duct indices
0 : Ambient quantity
c : Combustor section
conv : Convection
in : Inlet
max : Maximum
mean : Mean value
T : Total

## References

[1] J. G. Lee and D. A. Santavicca, Experimental diagnostics for the study of combustion instabilities in lean premixed combustors, *J. Propul. Power* 19 (2003) 735-750.

[2] T. Lieuwen and V. Yang, *Combustion instabilities in gas turbine engines*, Progress in Astronautics and Aeronautics, Vol. 210, AIAA, Washington, DC, (2005).

[3] S. Candel, Combustion dynamics and control: progress and challenges, *Proc. Combust. Instit*. 29 (2002) 1-28.

[4] R. Balachandran, B. O. Ayoola, C. F. Kaminski, A. P. Dowling and E. Mastorakos, Experimental investigation of the nonlinear response of turbulent premixed flames to imposed inlet velocity oscillations, *Combust. Flame* 143 (2005) 37-55.

[5] B. D. Bellows, Y. Neumeier and T. Lieuwen, Forced response of a swirling, premixed flame to flow disturbances, *J. Propul. Power* 22 (2006) 1075-1084.

[6] C. Kulsheimer and H. Buchner, Combustion dynamics of turbulent swirling flames, *Combust. Flame* 131 (2002) 70-84.

[7] T. Lieuwen and Y. Neumeier, Nonlinear pressure-heat release transfer function measurements in a premixed combustor, *Proc. Combust. Instit*. 29 (2002) 99-105.

[8] D. You, Y. Huang and V. Yang, A generalized model of acoustic response of turbulent premixed flame and its application to gas-turbine combustion instability analysis, *Combust. Sci. Technol*. 177 (2005) 1109-1150.

[9] M. Fleifil, A. M. Annaswamy, Z. A. Ghoneim and A. F. Ghoniem, Response of a laminar premixed flame to flow oscillations: a kinematic model and thermoacoustic instability results, *Combust. Flame* 106 (1996) 487-510.

[10] S. H. Preetham and T. Lieuwen, Response of turbulent premixed flames to harmonic acoustic forcing, *Proc. Combust. Instit*. 31 (2007) 1427-1434.

[11] C. A. Armitage, R. Balachandran, E. Mastorakos and R. S. Cant, Investigation of the nonlinear response of turbulent premixed flames to imposed inlet velocity oscillations, *Combust. Flame* 146 (2006) 419-436.

[12] A. X. Sengissen, J. F. Van Kampen, R. A. Huls, G. G. M. Stoffels, J. B. W. Kok and T. J. Poinsot, LES and experimental studies of cold and reacting flow

in a swirled partially premixed burner with and without fuel modulation, *Combust. Flame* 150 (2007) 40-53.

[13] A. Gentemann, C. Hirsch, K. Kunze, F. Kiesewetter, T. Sattelmayer and W. Polifke, Validation of flame transfer function reconstruction for perfectly premixed swirl flames, *Proceedings of ASME Turbo Expo*, Vienna, Austria, June 14-17, 2004.

[14] N. Noiray, D. Durox, T. Schuller and S. Candel, Self-induced instabilities of premixed flames in a multiple injection configuration, *Combust. Flame* 145 (2006) 435-446.

[15] V. Bellucci, B. Schuermans, D. Nowak, P. Flohr and C. O. Paschereit, Thermoacoustic modeling of a gas turbine combustor equipped with acoustic dampers, *J. Eng. Gas Turb. Power* 127 (2005) 372-379.

[16] Y. Huang and W. T. Baumann, Reduced-order modeling of dynamic heat release for thermoacoustic instability prediction, *Combust. Sci. Technol*. 179 (2007) 617-636.

[17] N. Ananthkrishnan, S. Deo and F. E. C. Culick, Reduced-order modeling and dynamics of nonlinear acoustic waves in a combustion chamber, *Combust. Sci. Technol*. 177 (2005) 221-247.

[18] T. J. Poinsot and D. P. Veynante, *Theoretical and Numerical Combustion*, 2nd ed. Edwards, Ann Arbor, MI, (2005).

[19] M. P. Waser and M. J. Crocker, Introduction to the two-microphone cross-spectral method of determining sound intensity, *Noise Control Eng. J*. 22 (1984) 76-85.

[20] M. Abom and H. Boden, Error analysis of two-microphone measurements in ducts with flow, *J. Acoust. Soc. Am*. 83 (1988) 2429-2438.

[21] W. Polifke, A. Poncet, C. O. Paschereit and K. Dobbeling, Reconstruction of acoustic transfer matrices by instationary computational fluid dynamics, *J. Sound Vib*. 245 (2001) 483-510.

[22] D. Kim, J. G. Lee, B. D. Quay and D. A. Santavicca, Effect of flame structure on the flame transfer function in a premixed gas turbine combustor, *Proceedings of ASME Turbo Expo*, Berlin, Germany, June 9-13, 2008.

[23] B. D. Bellows, M. K. Bobba, A. Forte, J. M. Seitzman and T. Lieuwen, Flame transfer function saturation mechanisms in a swirl-stabilized combustor, *Proc. Combust. Instit*. 31 (2007) 3181-3188.

[24] D. Durox, F. Baillot, G. Searby and L. Boyer, On the shape of flames under strong acoustic forcing: a mean flow controlled by an oscillating flow, *J. Fluid Mech*. 350 (1997) 295-310.

[25] A. P. Dowling, Nonlinear self-excited oscillations of a ducted flame, *J. Fluid Mech*. 346 (1997) 271-290.

[26] A. A. Peracchio and W. M. Proscia, Nonlinear heat release/acoustic model for thermo-acoustic instability in lean premixed combustors, *J. Eng. Gas Turb. Power* 121 (1999) 415-421.

[27] K. T. Kim, J. G. Lee, H. J. Lee, B. Quay and D. A. Santavicca, Characterization of forced flame response of swirl-stabilized turbulent lean-premixed flames in a gas turbine combustor, *Proceedings of ASME Turbo Expo*, Orlando, FL, USA, June 8-12, 2009.

[28] M. C. Garcia, E. Mastorakos and A. P. Dowling, Investigations on the self-excited oscillations in a kerosene spray flame, *Combust. Flame* 156 (2009) 374-384.

[29] T. Lieuwen, V. McDonell, D. A. Santavicca and T. Sattelmayer, Burner development and operability issues associated with steady flowing syngas fired combustors, *Combust. Sci. Technol*. 180 (2008) 1167-1190.

[30] H. Buchner, C. Hirsch and W. Leuckel, Experimental investigation on the dynamics of pulsated premixed axial jet flames, *Combust. Sci. Technol*. 94 (1993) 219-228.

[31] N. Noiray, D. Durox, T. Schuller and S. Candel, A unified framework for nonlinear combustion instability analysis based on the flame describing function, *J. Fluid Mech*. 615 (2008) 139-167.

**Kyu Tae Kim** is a research associate at the department of engineering in the University of Cambridge. He received his Ph.D. degree at the department of mechanical and nuclear engineering in the Pennsylvania State University, 2009. His research interest includes thermoacoustic instabilities in lean premixed gas turbine engines, hydrogen combustion, and nonlinear stability analysis.